Rare Metal Materials and Engineering
Volume 55, Issue 8, August 2026
Available online at www.rmme.ac.cn

Science Press

Cite this article as: Liu Xiaoyu, Zhi Lei, Xia Haoyu, et al. Synthesis and Performance Characterization of Mo_2BC Bulk Prepared by Spark Plasma Sintering [J]. Rare Metal Materials and Engineering, 2026, 55(08): 1889-1896. DOI: https://doi.org/10.12442/j.issn.1002-185X.20250540.

ARTICLE

Synthesis and Performance Characterization of Mo_2BC Bulk Prepared by Spark Plasma Sintering

Liu Xiaoyu[1,2], Zhi Lei[2], Xia Haoyu[2], Feng Gong[2], Shao Botao[2], Liu Jing[2], Zhang Shengnan[2], Li Jianfeng[2], Zhang Pingxiang[2]

[1] School of Materials Science and Engineering, Northeastern University, Shenyang 110819, China; [2] Superconducting Materials Research Center, Northwest Institute for Nonferrous Metal Research, Xi'an 710016, China

Abstract: The high-purity Mo_2BC bulk was synthesized via spark plasma sintering (SPS) technique. Results show that the Mo_2BC bulk prepared by optimized SPS process exhibits exceptional structural homogeneity, with a Vickers hardness of 19 GPa. This considerable mechanical hardness is attributed to the strong covalent bonding network within the Mo_2BC crystal structure. Simultaneously, magnetic and electrical characterization confirms that the Mo_2BC bulk has superconductivity with a transition temperature of 7.8 K and a high upper critical field of 6.3 T. The coexistence of such notable mechanical properties and robust superconducting characteristics in Mo_2BC bulk reveals a promising candidate for advanced applications under extreme conditions. This study not only provides crucial insights into the non-centrosymmetric bulk materials, but also establishes SPS as an efficient route for developing novel superconductors with high hardness.

Key words: molybdenum borocarbide; high purity; high hardness; Type-II superconductor

1 Introduction

The exploration of new superconducting materials has been a major objective in condensed matter physics for decades, motivated by both fundamental scientific interest and potential applications. Among the various of superconductors, intermetallic compounds, particularly ternary boride-carbides[1–4], have recently attracted significant attention due to their unique crystal structures, which often exhibit high hardness, excellent chemical stability, and intriguing superconducting properties[5–8].

As the representative of molybdenum-rich ternary boride-carbides, Mo_2BC typically exhibits layered and non-centrosymmetric crystal structure, which is intrinsically linked to its superconducting behavior[9–11]. The crystal structure of Mo_2BC exhibits a highly distinctive and robust framework, constructed by two-dimensional layers of edge-sharing [Mo_6C] octahedra interconnected via zigzag chains of boron atoms. This specific configuration creates a three-dimensional network, in which the covalent bonds and metallic bonds coexist. The strong covalent bonds exist within the boron chains and between the boron and molybdenum/carbon atoms, providing exceptional structural stability. While the metallic bonds within the [Mo_6C] octahedra layers facilitate electrical conductivity[10]. This interplay between localized covalent bonds and delocalized metallic electrons, all within a non-centrosymmetric arrangement, is the fundamental origin of its excellent superconducting behavior. Furthermore, the inversion symmetry is absent in the Mo_2BC superconductor, leading to unconventional superconducting properties, such as the potentially topologically non-trivial superconducting phases[12–13]. Therefore, Mo_2BC can serve as an ideal platform for exploring the relationship between crystal structure, electronic band structure, and superconductivity.

Escamilla et al[14] fabricated a polycrystalline sample of Mo_2BC by arc-melting method using Mo_2B and carbon as precursors. The obtained sample exhibits a superconducting

Received date: October 20, 2025
Foundation item: Supported by Northwest Institute for Nonferrous Metal Research (YK2110); National Natural Science Foundation of China (52172274)
Corresponding author: Zhi Lei, Ph. D., Professor, Superconducting Materials Research Center, Northwest Institute for Nonferrous Metal Research, Xi'an 710016, P. R. China, E-mail: zleidcn@163. com; Li Jianfeng, Ph. D., Professor, Superconducting Materials Research Center, Northwest Institute for Nonferrous Metal Research, Xi'an 710016, P. R. China, E-mail: jfli@c-nin.com

transition temperature (T_c) value of 7.2 K and a low superconducting volume fraction of 12%. This reduced fraction can be attributed to the presence of more lattice defects in the sample, which enhance the strong flux pinning and lead to underestimation of superconducting volume. The X-ray photoelectron spectrometer (XPS) results revealed that the Mo 4d state of Mo_2BC significantly contributes to the electronic density of states (DOS) at the Fermi level. Furthermore, the electron-phonon coupling of Mo_2BC indicated that they are intermediate-coupled superconductor. Falconi et al[15] also synthesized Mo_2BC bulk by arc-melting technique and studied the electronic band structure of Mo_2BC under high pressure. With the increase in pressure to 5 GPa, a non-linear reduction of T_c can be observed in the electrical resistivity measurements. This phenomenon can be explained by the enhanced bandwidth of Mo_2BC under pressure, leading to a decrease in total DOS at the Fermi level. Ge et al[10] adopted high pressure and high temperature (HPHT) method to synthesize Mo_2BC by using molybdenum powder, carbon powder, and boron powder as precursors. HPHT process was conducted at a pressure of 5 GPa and a temperature range of 1400–2300 K. Their results depicted that a T_c of 7.0 K and an upper critical field of 4.3 T can be achieved in Mo_2BC bulk. The specific thermal tests indicated that a Debye temperature of 565.1 K and an electron-phonon coupling parameter of 0.558 can be fitted, suggesting it is a Bardeen-Cooper-Schrieffer (BCS) conventional superconductor. Saib et al[12] investigated the physical properties and superconductivity of orthorhombic Mo_2BC by using *Ab initio* pseudopotential calculations. The structural, electronic, elastic, mechanical, and electron-phonon interactions were investigated in detail. The results revealed that the nature of bonding in Mo_2BC is a combination of covalent, metallic, and ionic bonding. The dynamical stability of Mo_2BC was identified by the lattice dynamical calculations. Furthermore, a high T_c of 7.41 K was calculated, which is comparable to the experimental value.

Herein, an alternative and efficient synthesis route for Mo_2BC bulk via spark plasma sintering (SPS) technique was proposed, aiming to optimize its microstructure, phase purity, and superconducting properties. By optimizing the sintering temperature of 1400 ℃, the maximum heater power of 95%, the applied pressure of 40 MPa, and the holding time of 20 min, the highly dense and high purity Mo_2BC bulk was prepared. This study aims to underscore the efficacy of SPS as an advanced processing technique for optimizing the superconducting properties of Mo_2BC, with potential applications for other transition metal borocarbides.

2 Experiment

The Mo_2BC bulk was synthesized by SPS. The molybdenum powder (99.99%), boron powder (99.99%), and carbon powder (99.99%) with a molar ratio of 2:1:1 were used as precursor materials. The precursor mixture was ground in an agate mortar for 30 min to achieve homogeneity. The resulting powder was then pressed into a graphite mold with an inner diameter of 13 mm. SPS process was conducted based on a factorial design under a constant pressure of 40 MPa and a holding time of 20 min. Three samples were fabricated with the following parameters: sample 1 (1300 ℃, heater power of 75%), sample 2 (1400 ℃, heater power of 75%), and sample 3 (1400 ℃, heater power of 95%). After cooling, the sintered samples were polished on both sides to remove surface impurities, yielding the final Mo_2BC bulk products.

The crystal structure of samples was characterized with a DX2700 X-ray diffractometer (XRD) with Cu Kα radiation (λ=0.154 06 nm, 40 kV). XRD patterns were analyzed using a Rietveld refinement. The morphologies of the samples were analyzed by a field emission scanning electron microscope (SEM, Hitachi 6700). XPS spectra of the sample were measured by AXIS ULTRA spectrometer (Kratos Analytical) employing a 100 μm monochromatic Al Kα X-ray beam (1486.71 eV) to irradiate the sample surface. Before the measurements, the sample was treated by Ar^+ sputtering for 10 min with a beam energy of 4 eV. The binding energy was calibrated by the adventitious C 1s peak at 284.8 eV. Before the quantification and peak fitting, the background contributions were subtracted using a Shirley function. The intensity ratios of the Mo $3d_{5/2}$ and $3d_{3/2}$ peaks were constrained to be 3:2. Vickers hardness was conducted on a micro-indentation Vickers hardness test (HV-1000ZDT). The magnetic and electrical transport properties of the samples were measured on a physical properties measurement system (PPMS, Quantum Design).

3 Results and Discussion

3.1 Microstructure

Fig.1a displays XRD patterns of the as-synthesized Mo_2BC bulk samples, suggesting the critical role of sintering temperature in determining the phase purity. In sample 1, two distinct impurity peaks at 26.6° and 28.0° can be assigned to unreacted carbon (C) and a molybdenum boride phase (Mo_4B), respectively. For sample 1, a sintering temperature of 1300 ℃ appears to be thermodynamically or kinetically insufficient to drive the solid-state reaction to completion. At this temperature, the atomic diffusion rates may be too low, leading to incomplete consumption of the starting materials (C and Mo_4B), and preventing the formation of a single-phase Mo_2BC compound. With the increase in sintering temperature to 1400 ℃, a significant improvement in phase formation is observed; however, a minor but detectable carbon peak persists, suggesting that the reaction is still not fully complete under these specific power conditions. In contrast, XRD patterns for sample 3 can be well indexed to the standard reference for the pure Mo_2BC phase, with no detectable secondary phases. This demonstrates that achieving complete phase purity requires not only a sufficient sintering temperature to drive the reaction thermodynamics but also an adequate power input to ensure favorable kinetics, possibly through enhanced Joule heating and diffusion. The sintering temperature of 1400 ℃ and a high power input are essential for the preparation of single-phase Mo_2BC. Moreover, the

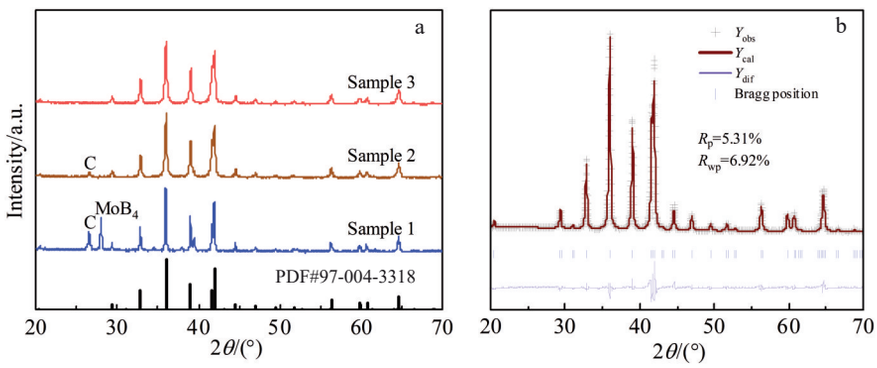

Fig.1 XRD patterns of different Mo_2BC bulk samples (a) and Rietveld refinement of XRD pattern for Sample 3 (b)

Rietveld refinement of XRD pattern for sample 3 (Fig. 1b) confirms that the synthesized Mo_2BC exhibits orthorhombic structure with the space group *Cmcm* (No. 63) [15], demonstrating high phase purity and excellent structural quality. XRD pattern shows an excellent match between the observed data (Y_{obs}) and the calculated profile (Y_{cal}) for the Mo_2BC phase, as evidenced by the minimal deviation in the difference curve (Y_{dif}). All the diffraction peaks are exclusively indexed to the Mo_2BC structure, with no residual impurity peaks such as unreacted C or Mo_4B, which are present in the sample 1. As shown in Table 1, the refined lattice parameters of the SPS-synthesized sample are a=0.309 06 nm, b=1.735 03 nm, and c=0.305 12 nm. Compared with the standard crystallographic data (PDF#97-004-3318), these values reveal a distinct anisotropic lattice expansion. Specifically, the *a*- and *c*-axes exhibit a noticeable enlargement, whereas the *b*-axis remains virtually unchanged. This phenomenon is attributed to the highly anisotropic layered structure of Mo_2BC, where the expansion primarily occurs within the covalent-bonded basal planes. Along the *b*-axis direction, the strong covalent bonds formed by the B-B atomic chains exhibit extremely high stability and compressibility resistance. Under high temperature and high pressure, their thermal expansion effect and pressure sensitivity are relatively low, resulting in minimal changes in the *b*-axis lattice parameters. In contrast, the *a*-*c* plane consists of Mo_6C octahedral layers, where the metallic bonding characteristics between Mo-Mo atoms make the bonding relatively softer and more ductile. This leads to more significant changes in the *a*- and *c*-axes lattice parameters under high temperature and high pressure. Consequently, the lattice anisotropy results in mechanical anisotropy, causing differences in compressive strength along the *b*-axis and the *a*-*c* plane. Furthermore, the localized stresses generate, which are induced by the anisotropic lattice distortions within the grains or at grain boundaries, thereby affecting the fracture toughness and long-term reliability.

Fig.2 exhibits SEM images of sample 2 and sample 3. The low-magnification SEM image of sample 2 sintered with 75% power (Fig. 2a) displays a microstructure with residual porosity, suggesting incomplete densification. A higher-magnification image (Fig.2b) further confirms the presence of

Table 1 Refined lattice parameters of sample 3 obtained from the Rietveld refinement

Parameter	Mo_2BC
Formula weight	214.70
Radiation	Cu Kα
Wavelength/nm	0.154 06
Space group	*Cmcm* (No.63)
Unit cell dimension/nm	a=0.309 06
	b=1.735 03
	c=0.305 12
	$\alpha=\beta=\gamma=90°$
Volume/$\times10^{-3}$ nm^3	163.623 8
Density/g·cm^{-3}	8.716
2θ/(°)	20–70
Residual	R_p=5.31%
	R_{wp}=6.92%

fine-grained microstructure. The individual grain size is predominantly 1 – 3 μm, and grain boundaries appear less distinct. In contrast, the sample 3 sintered with 95% power (Fig. 2c) shows a significantly denser structure, which has fewer and smaller pores. Fig. 2d further demonstrates substantial grain growth, with grain size exceeding 3 – 6 μm. The grain boundaries are well-defined and sharp, forming a continuous and dense network. Based on the Archimedes method, using a theoretical density value of 8.74 g/cm^3 for Mo_2BC, the relative densities of sample 2 and sample 3 were calculated as 80.2% and 93.4%, respectively. The enhanced densification observed in sample 3 can be attributed to the intensified plasma activation and higher Joule heating, which promotes the atomic diffusion and mass transport, thereby enabling more effective reduction of pores and diminishing internal defects in the material. As pores act as internal defects and stress concentration points in the material, their reduction enhances the structural continuity of the sample, allowing stress to be distributed more uniformly. This enables the material to withstand higher loads, ultimately resulting in improved strength and hardness.

The elemental valence band states and surface chemical conditions of the sample 3 were examined by XPS. Prior to

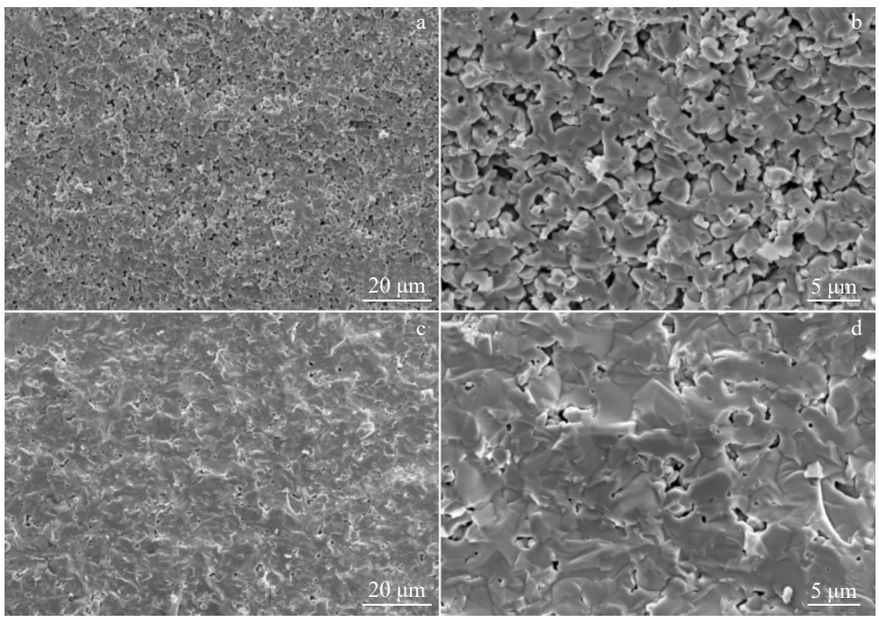

Fig.2 SEM images of sample 2 (a–b) and sample 3 (c–d) under different magnifications

XPS analysis, the Mo_2BC bulk was subjected to Ar^+ ion etching to eliminate the surface oxide layer, thereby ensuring that the collected signals originate from the pristine bulk material. Fig. 3a reveals the presence of the constituent elements of Mo, B, and C through their core-level peaks, including Mo 3p, Mo 3d, C 1s, and B 1s peaks. Besides, a minor O 1s peak is observed, which may originate from the surface adsorption or residual contaminants, as commonly seen even after etching[13]. Notably, there are almost no additional peaks appeared in the patterns, demonstrating a high phase purity, which agrees well with XRD results in Fig. 1b. The high-resolution Mo 3d spectrum shown in Fig. 3b displays a group of doublet peaks, which can be assigned as Mo $3d_{5/2}$ (228.72 eV) and Mo $3d_{3/2}$ (231.86 eV). The group of doublet peaks is characteristic of Mo^{2+}, which is consistent with its bonding in the ternary Mo_2BC compound. Moreover, the absence of Mo^{4+} and Mo^{6+} peaks indicates that the successful elimination of high oxidation states of MoO_2 and MoO_3[16–19]. This further confirms the efficacy of the Ar^+ ion etching process in revealing the intrinsic electronic structure. The high-resolution of C 1s peak depicted in Fig. 3c can be deconvoluted into two peaks. The dominant peak at 283.86 eV

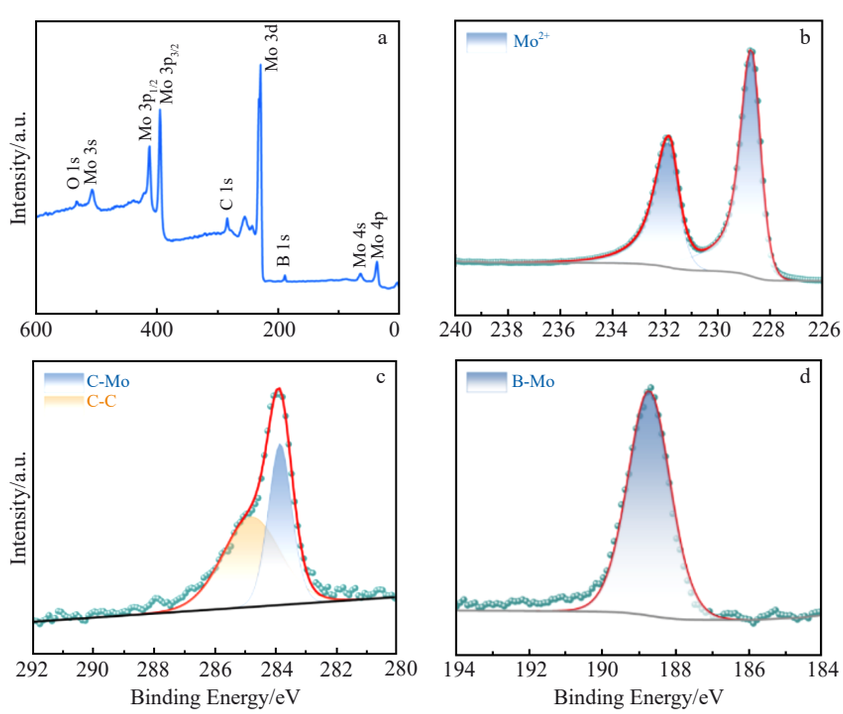

Fig.3 Full XPS spectrum (a) and high-resolution XPS spectra of Mo 3d (b), C 1s (c), and B 1s (d) of sample 3

is assigned to C-Mo bonding, which is a characteristic signature of the carbide phase in Mo_2BC. In the B 1s spectrum (Fig. 3d), a single peak appears at 188.72 eV, which is typical for B-Mo bonding in transition metal borides. It is noted that no substantial C-O or B-O species can be observed in Fig. 3c and Fig. 3d, further validating the effectiveness of Ar^+ ion etching in removing surface oxides.

3.2 Nanoindentation hardness

Fig. 4 illustrates the variation of hardness with applied load for the Mo_2BC bulk, as measured by micro-indentation Vickers hardness. A distinct trend is observed. As the applied load increases from 0.49 N to 9.80 N, the hardness exhibits a gradual decrease from approximately 19.2 GPa to 19.0 GPa. This behavior is a clear manifestation of the indentation size effect, which is commonly observed in hard bulk materials[20–22]. At lower loads, the indentation volume is small and confined to a region strongly influenced by surface interactions, strain gradient plasticity, and the initial elastic-plastic transition, leading to an apparently higher hardness. As the indentation load increases, the indentation involves a larger material volume that is more representative of the intrinsic properties of the bulk, resulting in a stable and slightly lower hardness value. The relatively small variation in hardness over the load range can be attributed to the high structural integrity and homogeneous microstructure of the Mo_2BC bulk. By SPS, the three-dimensional covalent network with a high relative density is achieved in the Mo_2BC bulk, providing consistent resistance to deformation across different applied loads. The chemical bonding in Mo_2BC is a combination of covalent, ionic, and metallic bonds. Specifically, covalent bonds (B-B, Mo-C) provide hardness and strength. The compressive strength along the *b*-axis and *c*-axis directions is attributed to the B-chains formed by strong covalent bonds between boron atoms, while the compressive strength along the *a*-axis direction is attributed to the Mo_6C octahedral layers. The interlocking of Mo_6C octahedra with two-dimensional B-chains creates a structure that can effectively prevent the sliding of B-chains under external stress while simultaneously restricting relative displacement between the Mo_6C octahedral layers. This synergistic reinforcement mechanism enables Mo_2BC to achieve high bulk modulus, high shear modulus, and exceptional hardness. The ionic bonds (Mo-B), characterized by strong electrostatic attraction, significantly enhance the cohesion of the entire three-dimensional network, thereby improving structural stability and bulk modulus. The metallic bonds (Mo-Mo), which are non-directional, allow atoms to slip through dislocation motion and rearrangement under stress, enabling a certain degree of toughness. This unique bonding characteristic makes Mo_2BC a highly promising ceramic material[23–25].

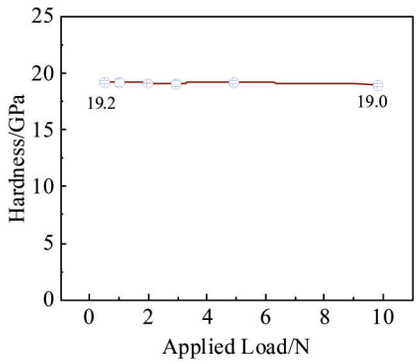

Fig.4 Variation of micro-indentation Vickers hardness of sample 3 with applied load

3.3 Superconducting properties

Fig. 5a exhibits the temperature-dependent magnetic susceptibility of sample 3 measured under zero-field cooling (ZFC) and field cooling (FC) mode with an applied magnetic field strength of H=795.77 A/m. The superconducting transition is characterized by three key temperatures: the onset transition temperature (T_c^{onset}), the critical temperature (T_c), and the offset temperature (T_c^{offset}). The T_c^{onset} is determined from the ZFC curve by identifying the point where the data begin to deviate from the normal-state baseline, the T_c is defined as the crossing point between the extrapolation of the normal state and the drop, and the T_c^{offset} is identified at the point where the curve levels off, suggesting the completion of the transition into a fully superconducting state[26–29]. It is noted that the T_c^{onset} and T_c values are identical, yielding a high T_c value of 7.6 K. Furthermore, ZFC curve exhibits an exceptionally sharp transition, with a T_c^{offset} value of 7.4 K. The extremely narrow transition of 0.2 K indicates the high chemical homogeneity and phase purity of the sample. Fig. 5b illustrates the *M-H* curves of Mo_2BC recorded at 3.0 and 6.0 K. *M* means magnetization. The observed clear hysteresis loops reveal that Mo_2BC is a typical type-II superconductor, where magnetic flux can penetrate the material in the form of quantized vortices, leading to the irreversible magnetic behavior. To quantify the lower critical field H_{c1}, the *M-H* curves of Mo_2BC were recorded from 2.0 to 6.5 K, as depicted in Fig. 5c. The H_{c1} is determined from the deviation from the linear line with a slope of – 1.0 at each temperature. The following temperature-dependence of H_{c1} is plotted in Fig. 5d. By fitting the $H_{c1}(T)$ data using the Werthamer-Helfand-Hochenberg (WHH) model, $\mu_0 H_{c1} = \mu_0 H_{c1}(0)[1-(T/T_c)^2]$, where μ_0 is the vacuum permeability (a fundamental physical constant). The extrapolated $H_{c1}(0)$ is determined to be 16 870.43 A/m. The electronic transport properties of Mo_2BC were examined by measuring its electrical resistivity using the four-probe method.

Fig. 6a shows the temperature dependence of resistivity (ρ-T) curve of sample 3 in zero magnetic field, which exhibits excellent metallic behavior in the normal state, characterized by a decreasing resistivity with the decrease in temperature. A sharp and well-defined superconducting transition is observed, with the resistivity dropping abruptly to zero at a critical temperature of T_c=7.8 K. Additionally, the narrow transition width confirms the high sample quality and phase purity, which is consistent with the magnetic susceptibility measurements shown in Fig. 5a. Fig. 6b illustrates the

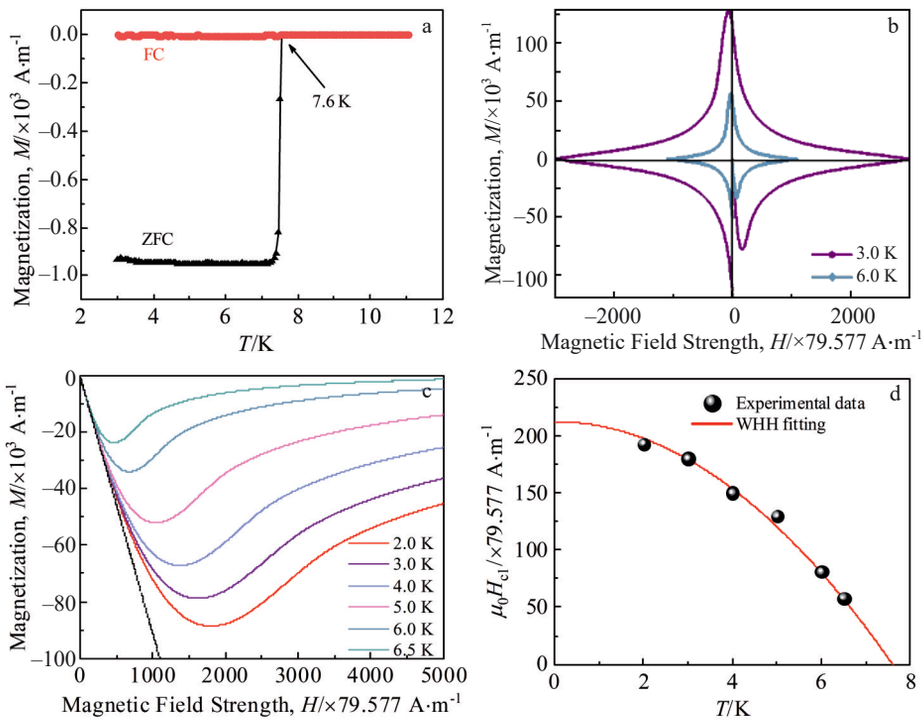

Fig.5 Magnetic susceptibility measurements of sample 3: (a) *M-T* plots recorded in ZFC and FC modes (*H*=795.77 A/m), (b) *M-H* loops recorded at 3.0 and 6.0 K, (c) *M-H* loops recorded from 2.0 K to 6.5 K, and (d) $\mu_0 H_{c1}$-*T* curve fitted with WHH model

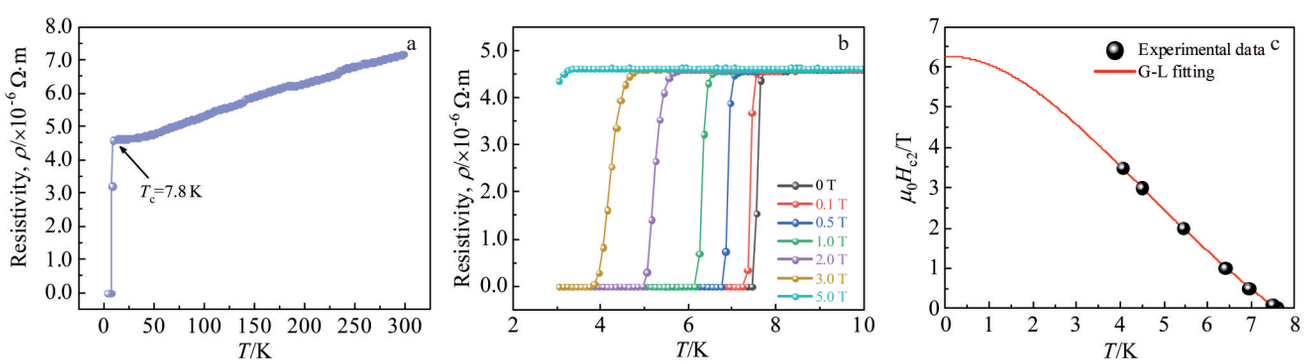

Fig.6 Resistivity measurements of sample 3: (a) ρ-*T* curve; (b) ρ-*T* curves in a magnetic field range of 0–5.0 T; (c) $\mu_0 H_{c2}$-*T* curve fitted by obtaining data at 90% of T_c from the ρ-*T* plots using G-L model

resistivity under an applied magnetic field. A clear suppression of T_c is observed with the increase in magnetic field, and the superconducting transition is almost completely suppressed at a field of 5.0 T. The temperature dependence of the upper critical field $H_{c2}(T)$, is determined from these transitions and fitted with Ginzburg-Landau (G-L) model.

$$\mu_0 H_{c2}(T) = \mu_0 H_{c2}(0)\left\{\left[1-(T/T_c)^2\right]/\left[1+(T/T_c)^2\right]\right\} \quad (1)$$

The excellent agreement between the experimental data and the G-L model confirms that Mo_2BC indicates a type-II superconducting behavior. Based on the fitting results, the upper magnetic field $H_{c2}(0)$ is determined to be 6.3 T. This value provides crucial insight into the stability of the superconducting state and suggests the potential of Mo_2BC for applications in high-magnetic-field environments. The G-L coherence length (ξ_{GL}) is calculated using Eq.(2).

$$H_{c2}(0) = \Phi_0/2\pi\xi_{GL}^2 \quad (2)$$

where Φ_0 represents the magnetic flux quantum, and the value is 2.067 8×10^{-15} T·m^2. By using the $H_{c2}(0)$=6.3 T, the $\xi_{GL}(0)$ were calculated as 7.2 nm. The penetration depth λ can be expressed as follows:

$$H_{c1}(0) \approx \Phi_0/4\pi\lambda^2 \ln(\lambda/\xi_{GL}) \quad (3)$$

By substituting $\xi_{GL}(0)$ =7.2 nm into Eq. (3), the λ of 154.3 nm was obtained. Consequently, a G-L parameter $\kappa = \lambda/\xi_{GL}$ = 21.4 was derived. This value significantly exceeds $1/\sqrt{2}$, unequivocally classifying Mo_2BC as a strong type-II superconductor[9]. The relatively short coherence length and large penetration depth are consistent with the observed higher upper critical field, and place Mo_2BC in the same category as

other well-known type-II superconductors, such as Nb_3Sn and MgB_2, which are recognized for their potential in high-field applications.

The origin of superconductivity lies in the electronic states near the Fermi level, which are dominated by the 4d orbitals of molybdenum. The strong hybridization between Mo atoms and the covalent B-C chains leads to a high electronic DOS at the Fermi level. According to BCS theory, a high DOS is crucial for achieving a high T_c, as it enhances the formation of Cooper pairs via the electron-phonon coupling mechanism. In Mo_2BC, the vibrational modes involving Mo atoms and the stretching modes of the B-C chains provide an effective pathway for this coupling, facilitating the emergence of superconductivity.

Mo_2BC, which uniquely integrates high hardness and superconducting performance, has emerged as a structural-functional material with broad applications. In future nuclear fusion applications[30–31], the stable 3D covalent network of Mo_2BC contributes to excellent radiation resistance. Meanwhile, its relatively high upper critical field enables it to maintain superconductivity under a strong magnetic field, while its high hardness can effectively resist the Lorentz forces, thereby significantly extending the service life of the critical components. In extreme high-pressure devices, Mo_2BC can serve as high-pressure electrical contact components; its superconducting properties ensure zero-resistance signal transmission in low-temperature and high-pressure environments, while its high hardness prevents deformation or fracture under GPa-level pressures, making it suitable for key components such as micro-electrodes in high-pressure chambers. This study significantly improves the hardness and superconductivity of Mo_2BC, laying a crucial foundation for its practical applications in extreme service environments.

4 Conclusions

1) The Mo_2BC bulk material was prepared via the optimized SPS technique with a sintering temperature of 1400 ℃, the maximum heater power of 95%, an applied pressure of 40 MPa, and a holding time of 20 min. These specific parameters are crucial for achieving the desired high phase purity and densification, which directly contribute to the superior mechanical properties.

2) The Mo_2BC bulk material prepared by SPS exhibits superior structural homogeneity and high relative density, which collectively contribute to its outstanding intrinsic hardness. The remarkable mechanical hardness arises from the rigid and three-dimensional covalent network formed by the B-C chains within the Mo matrix.

3) The Mo_2BC bulk material exhibits a sharp bulk superconducting transition with a T_c of 7.8 K, as confirmed by both resistivity and magnetization measurements. Through the analysis, the upper critical field (H_{c2}) of Mo_2BC bulk material is determined to be 6.3 T. The as-calculated G-L coherence length $\xi_{GL}(0)$ is 7.2 nm and the magnetic penetration depth $\lambda(0)$ is 154.3 nm. The resulting G-L parameter is κ=21.4, which is much larger than the threshold of $1/\sqrt{2}$, definitively confirming its strong type-II character.

References

1 Pickett W E. *Journal of Physics*[J], 2003, 33: 695

2 Haque E, Hossain M A, Stampfl C *et al. Physical Chemistry Chemical Physics*[J], 2019, 21: 8767

3 Miao R D, Huang G Q, Yang J *et al. Solid State Communications*[J], 2016, 233: 30

4 Wang J N, Yan X W, Gao M *et al. Physical Review B*[J], 2021, 103: 144515

5 Bolvardi H, Emmerlich J, To Baben M *et al. Journal of Physics: Condensed Matter*[J], 2013, 25: 045501

6 Lejay P, Chevalier B, Etourneau J *et al. Synthetic Metals*[J], 1981, 4: 139

7 Lejay P, Chevalier B, Etourneau J *et al. Journal of the Less Common Metals*[J], 1981, 82: 193

8 Cao L K, Yang F, Shi J T *et al. Rare Metal Materials and Engineering*[J], 2025, 54(10): 2671

9 Bovin J O, O'Keeffe M, Stenberg L. *Journal of State Chemistry*[J], 1977, 22: 221

10 Ge Y F, Zhou C, Wang N N *et al. International Journal of Refractory Metals and Hard Materials*[J], 2024, 123: 106757

11 Wang S, Pang X J, Zhang Z Y *et al. Journal of the European Ceramic Society*[J], 2021, 41: 5109

12 Saib S, Uzunok H Y, Karaca E *et al. Journal of Applied Physics*[J], 2021, 130: 153902

13 Barua P, Hossain M M, Ali M A *et al. Journal of Alloys and Compounds*[J], 2019, 770: 523

14 Escamilla R, Carvajal E, Cruz-Irisson M *et al. Journal of Materials Science*[J], 2016, 51: 6411

15 Falconi R, De La Mora P, Morales F *et al. Journal of Low Temperature Physics*[J], 2015, 179: 158

16 Zhang Z Y, Wang S, Pang X J *et al. Journal of Alloys and Compounds*[J], 2023, 965: 171335

17 Xia H Y, Zhi L, Feng G *et al. Journal of Physics and Chemistry of Solids*[J], 2024, 193: 112163

18 Zhi L, Xia H Y, Feng G *et al. Journal of Physics and Chemistry of Solids*[J], 2025, 199: 112560

19 Halim J, Kota S, Lukatskaya M R *et al. Advanced Functional Materials*[J], 2016, 26: 3118

20 Ge Y F, Bao K, Ma T *et al. ACS Omega*[J], 2021, 6: 21436

21 Emmerlich J, Music D, Braun M *et al. Journal of Physics D: Applied Physics*[J], 2009, 42: 185406

22 Ge Y F, Ma S L, Bao K *et al. Inorganic Chemistry Frontiers*[J], 2019, 6: 1282

23 Escamilla R, Carvajal E, Cruz-Irisson M *et al. Journal of Molecular Structure*[J], 2016, 1125: 350.

24 Liu Y Z, Jiang Y H, Zhou R *et al. Ceramics International*[J], 2015, 41: 5239

25 Liu Y Z, Sun L, Zhang B C *et al. Ceramics International*[J],

2021, 47: 1421
26 Zhang Z, Fang Y Q, Wang D *et al. Journal of Materials Chemistry C*[J], 2020, 8: 2682
27 Zhang J L, Cao Z, He X *et al. Journal of Physical Chemistry Letters*[J], 2021, 12: 2219
28 Kamysbayev V, Filatov A S, Hu H C *et al. Science*[J], 2020, 369: 979
29 Fan Y J, Xu C, Liu X *et al. NPG Asia Materials*[J], 2020, 12: 60
30 Yang Yihang, Yang Fang, Liu Jixing *et al. Rare Metal Materials and Engineering*[J], 2025, 54(9): 2395 (in Chinese)
31 Xing Bo, Hao Ziyan, Wang Pengfei *et al. Rare Metal Materials and Engineering*[J], 2025, 54(11): 2949 (in Chinese)

放电等离子烧结制备Mo_2BC块体及其性能表征

刘逍宇[1,2]，郅　磊[2]，夏昊宇[2]，冯　龚[2]，邵柏淘[2]，刘　静[2]，张胜楠[2]，李建峰[2]，张平祥[2]
(1. 东北大学 材料科学与工程学院，辽宁 沈阳 110819)
(2. 西北有色金属研究院 超导材料研究所，陕西 西安 710016)

摘　要：通过放电等离子烧结（SPS）制备出了高纯度的Mo_2BC块体。结果表明，经优化后的SPS工艺所制备出的Mo_2BC块体材料结构均匀性极高，维氏硬度达到19 GPa，这归功于Mo_2BC晶体结构内部的强共价键网络。磁学和电学表征证实该材料具有超导性能，超导转变温度为7.8 K，上临界场高达6.3 T。Mo_2BC中优异的力学性能与强超导特性的共存，使其成为极端条件下的理想候选材料。本研究不仅为非中心对称块体材料提供了重要见解，也确立了SPS制备高硬度新型超导体的有效技术路径。

关键词：硼碳化钼；高纯度；高硬度；第二类超导体

作者简介：刘逍宇，男，2001年生，硕士，东北大学材料科学与工程学院，辽宁 沈阳 110819，E-mail：15175905077@163.com